Journal of Cluster Science (2021) 32:209–219
https://doi.org/10.1007/s10876-020-01779-7

ORIGINAL PAPER

Gum Acacia Modified Ni Doped CuO Nanoparticles: An Excellent Antibacterial Material

Lalit Mohan Dwivedi[1] · Neelam Shukla[1] · Kirti Baranwal[1] · Surabhi Gupta[1] · Shehala Siddique[1] · Vandana Singh[1]

Received: 15 November 2019 / Published online: 25 March 2020

Abstract

Ni doped CuO Nps ($Ni_{0.1}$CuO-GA) grown in gum acacia (GA) medium behaved as an efficient antibacterial material. The antibacterial activity of $Ni_{0.1}$CuO-GA was much higher than the control antibiotic (Amplicillin) and simple Ni doped CuO Nps. Different concentrations of GA were used (as the growth medium) to tune the material's bioactivity. Among the synthesized $Ni_{0.1}$CuO-GA samples (G_1–G_4), G_3 sample (synthesized using 1.5% (w/v) GA) showed optimum antibacterial activity. The corresponding undoped sample (CuO-GA) was less active. The structural, morphological, compositional and optical properties of G_3 have been determined by FTIR, XRD, FESEM, HR-TEM and UV–visible analyses. It exhibited excellent antibacterial activity for *Enterobacter, Klebsiella pneumoniae, Pseudomonas aeruginosa* and *Staphylococcus aureus* bacterial strains (ZOI being 27 mm, 28.75 mm, 27.50 mm and 26.50 mm respectively). ZOI for the reference antibiotic for respective bacterial strains were 17.50 mm, 18.50 mm, 18.25 mm and 19.50 mm respectively, while ZOI for neat CuO Nps, G_1, G_2, G_4 and CuO-GA samples ranged between 21 and 24 mm for the same doses. The advantage Ni doping combined with the usage of GA as growth medium is evident by the excellent antibacterial behaviour of G_3.

Keywords Gum acacia · Nickel · CuO · Nanoparticles · Antibacterial activity

Introduction

Assemblies of hetero- or homo-nanostructures are of great interest [1] as they exhibit unusual physical, chemical and biological properties, different from the respective bulk materials [2]. The confluence of nanotechnology and biology has been utilized to address several biomedical issues [3]. Noble metal nanoparticles have been extensively investigated for their antibacterial effects [4]. Cu and CuO nanostructures are the economical alternatives of noble metal nanoparticles. Copper oxide is considered as one of the important metal oxide because of its low cost, abundant availability and peculiar properties. It is an important p-type transition metal oxide semiconductor material which has a narrow band gap of 1.2 eV. It finds use in photocatalytic and antibacterial applications [5], electrochemical sensors [6], light emitters [7], gas sensors [8], super capicitors [9], magnetic storage media [10], thermoelectric materials [11], photovoltaic cells [12], and catalysis [13]. Various physical and chemical routes are known for synthesizing CuO nanostructures such as reactive ion sputtering [14], electro deposition [15], pulsed laser evaporation [16], hydrothermal process [17], sonochemical synthesis [18], microwave combustion [19], and chemical methods [20], [21]. Amongst these techniques, the co-precipitation process has attracted substantial attention as this method is simple and cost effective. It requires low amounts of energy and can be carried out at ambient temperature.

CuO nanoparticles are also known to have antimicrobial properties [22]; however their efficacy depends upon the size, stability and concentration of the nanoparticles which can be tuned by using certain growth mediums. Copper oxide nanoparticles (CuO and Cu_2O) cause severe damage to the bacterial cell envelope. The toxicity of cuprous oxide (Cu_2O) is because of the formation of copper(I)–peptide complex while cupric oxide (CuO) generate free radicals that harm the bacterial cells [23].

✉ Vandana Singh
vschemau@gmail.com

[1] Department of Chemistry, University of Allahabad, Allahabad 211002, India

The antibacterial property of CuO nanoparticles has been attributed to their ability to produce reactive oxygen species (ROS) on exposure to water [24]. These nanoparticles are especially attractive for biomedical applications [25]. Polysaccharides, being nontoxic are attractive as growth medium for modulating the size of nanoparticles however their presence often masks the antibacterial activity of the nanoparticles. Our research group has recently used guar gum as growth medium for ZnO nanoparticles where it has been witnessed that presence of guar gum decreased the antibacterial effect of ZnO Nps though oxidized guar gum could significantly enhance it [26]. CuO nanoparticles synthesized using Karaya gum as template has also shown antibacterial behaviour [27].

At the same time, radical changes in optical, electrical, and biological properties of CuO Nps can be made by altering the electronic structure of CuO by metal doping. CuO has been doped with transition metals, such as Ti [28], Fe [29], Cd [30], Zn and Mn [31], [32]. However there are only very few reports on Ni-doped bulk and/or nanostructured CuO [33], [34]. Nickel-doped copper oxide has been prepared by layer by spin-coating process [35]. Ni doping to CuO Nps, synthesized through rapid solid reaction method exhibited reduced average crystallite size [36]. CuO-NiO nanoparticles have shown greater toxicity against *S. aureus* than and *E. coli* bacterial strains than the neat NiO nanoparticles [37]. In another study Ni doping increased the antibacterial activity of CuO Nps for *Staphylococcus aureus, Streptococcus pneumoniae, Escherichia coli* and *Klebsiella pneumoniae* bacterial strains [38]. It has also been reported that Ni doped copper oxide nanoparticles exhibit better magnetic properties than the undoped CuO Nps [39]. CuO nanoparticles have been crafted for many desired applications by Ni doping, as the doping tailors the optical properties of CuO [40]. These antibacterial magnetic nanomaterials have tremendous potential in biomedical field.

We could not find any report on the effect of Ni doping on the antibacterial properties of CuO grown in polysaccharide growth medium. Natural biopolymers are known for alleviating the toxicity of metal or metal oxide nanoparticles besides manipulating their size and stabilizing them [26], [41].

In the present study, in order to design an efficient antibacterial material with novel optical, electrical, magnetic and antibacterial properties, Ni has been doped to GA grown CuO nanoparticles. Gum acacia is highly branched polysaccharide, isolated from exudates of widely distributed and abundantly available trees of *Acacia senegal* and *Acacia seyal* [42]. The gum acacia polysaccharide is reported to possess capping and stabilizing effect on Cu Nps [43] but these nanoparticles have not been screened for their antibacterial properties. The use of polysaccharide is not yet reported for the synthesis of Ni doped CuO nanoparticles. The purpose of this study is to develop antibacterial material by using a biocompatible growth medium.

Methods

Synthesis of $Ni_{0.1}$CuO-GA Nps, $Ni_{0.1}$CuO Nps and CuO Nps

To synthesize $Ni_{0.1}$CuO-GA, 40 mL of $NiSO_4{\cdot}6H_2O$ (0.01 M) was added to 40 mL of $CuSO_4{\cdot}5H_2O$ (0.1 M) and the mixture was stirred for 0.5 h. To this mixture, 30 mL of GA solution (1% (w/v)) was added and the stirring was continued for another 0.5 h. The pH of the reaction mixture was adjusted to pH 10.1 by drop wise addition of 1 M NaOH solution and the mixture was further stirred for 1.5 h at room temperature. The resulting colloidal solution was aged at room temperature for 24 h and was centrifuged. The product thus obtained was washed well with ethanol and distilled water and was dried (at 40 °C in an electric oven). The dried product was calcined in air (for 1 h) at 400 °C (Yield 390.2 mg). Similarly $Ni_{0.1}$CuO nanoparticles and neat CuO nanoparticles were also prepared but in absence of GA and $NiSO_4{\cdot}6H_2O$ respectively (Yields were 360.5 and 330.7 mg respectively). The reaction volumes were adjusted by adding distilled water. The synthesis of $Ni_{0.1}$CuO-GA was optimized by varying the GA concentration from 0.5 to 2.0% (w/v) while fixed concentrations of copper sulfate and nickel sulfate were used (0.1 M and 0.01 M respectively). CuO-GA was synthesized under the condtions of G_3 but without Ni doping (Yield 368 mg). The selection of copper sulfate and nickel sulphate concentrations was based upon our trial experiments. All the synthesized samples (G_1 to G_4, CuO, CuO-GA, and $Ni_{0.1}$-CuO Nps) were screened for their antibacterial activity.

Characterization

UV–visible absorption measurements were carried out in the wavelength range of 200–800 nm on Shimadzu UV spectrophotometer (UV-1800) (Japan). The band gap was calculated by the tauc plot, $((\alpha h\nu)^2$ vs. $h\nu)$, where α is the absorption coefficient of the material and $h\nu$ denotes the photon energy. The materials were calcined in an electric muffle furnace (Metrex Scientific Instruments (P) Ltd., New Delhi). X-ray diffraction study (Cu $K\alpha$ source) was done (using powdered samples) on a Rigaku Smart Lab using Cu Kα ($\lambda = 1.54$ A) radiation. IR was done by forming KBr pallets through Spectrum 2 Perkin Elmer Spectrophotometer, within the spectral range of 450–4000 cm^{-1} and resolution 4 cm^{-1}. FE-SEM study

was performed using Nova Nano FE-SEM 450 (FEI) while TEM analysis was done on Tecnai G 2 20 (FEI) S-Twin 200 kV transmission electron microscope. The SEM sample was prepared by depositing a drop of the material's suspension on double stick carbon tape of aluminum stubs and was dried and coated with gold.

Antibacterial Activity

Antibacterial activities of the samples (G_1–G_4), CuO (1), $Ni_{0.1}CuO$ (2), CuO-GA (figure not shown) were evaluated against gram-negative (*Enterobacter, Klebsiella pneumoniae* and *Pseudomonas aeruginosa*) and gram-positive (*Staphylococcus aureus*) bacterial strains. The antibacterial activity test was performed by agar well diffusion method. In brief, 100 µL suspension of each bacterial strain (1.0×10^6 colony forming units/mL) was spread over nutrient agar plates with the help of a sterile glass-rod spreader. Plates were left for 10 min to let the culture get absorbed. Then 6 mm wells were punched (by using sterile cork borer) into the nutrient agar plates for testing antibacterial activity of the synthesized nanomaterials. The nanomaterial solution (100 µL of 5 mg/mL) in sterilized distilled water was poured into the wells (on all plates) with the help of a micropipette. The petri dishes were incubated for 16 h at 37 ± 0.2 °C and then the diameters of inhibition growth zones (ZOI) were measured. Solvent blank was used as negative control and antibiotic ampicillin (5 mg/mL) was used as a positive control. The study was done in triplicates and the average of three results is reported.

Results and Discussion

Ni (0.01 mol) was doped into GA grown CuO nanoparticles to obtain $Ni_{0.1}CuO$-GA samples (Scheme 1). The extent of Ni doping was chosen based upon our trial experiments where antibacterial activity of the product was targeted. The extent of GA was varied from 0.50% to 2.00% (w/v) at this formulation and the materials were calcined at 400 °C to obtain samples G_1 to G_4 respectively (Table 1).

In a preliminary study, all of the synthesized samples were evaluated for their antibacterial properties against gram positive (*S. aureus*) and gram negative (*P. aeruginosa*, *Enterobacter, K. pneumoniae*) bacterial strains. Among G_1 to G_4 samples, G_3 sample exhibited highest bioactivity for the studied bacterial strains therefore this sample was selected for detailed characterization and antibacterial study. Sample CuO-GA was synthesized (as G_3 but without Ni doping) to understand the effect of nickel doping on the antibacterial efficacy of the material. Similarly CuO (in absence of GA and Ni doping) and $Ni_{0.1}CuO$ controls (in absence GA) were also synthesized.

FTIR spectra of CuO, $Ni_{0.1}CuO$, G_3 and GA are presented in Fig. 1. In the FTIR spectrum of GA, O–H and C–H stretching vibrations are visible at 3299 cm^{-1} and 2935 cm^{-1} respectively. The asymmetric and symmetric stretching vibrations of COO^- are visible at 1601 cm^{-1} and 1367 cm^{-1} respectively [43]. The absorption band at 1021 cm^{-1} is due to C-O stretching.

The FTIR spectrum of CuO showed three characteristic strong peaks associated with the Cu–O vibrations of monoclinic CuO at 415 cm^{-1}, 483 cm^{-1} and 598 cm^{-1} [32]. The band located at ~ 483 cm^{-1} can be assigned to Cu–O stretching along (101) direction and that at about 598 cm^{-1} is associated with Cu–O stretching along (−101) direction [44] and no active bands at 630 cm^{-1} were seen, thus Cu_2O phase indicated by XRD peaks is only in traces [45]. The peaks observed at 1436 cm^{-1} and 1117 cm^{-1} can be attributed to O–H bending vibrations combined with metal atoms while the band located at 1041 cm^{-1} is because of C-O stretching vibrations. In FTIR spectra of

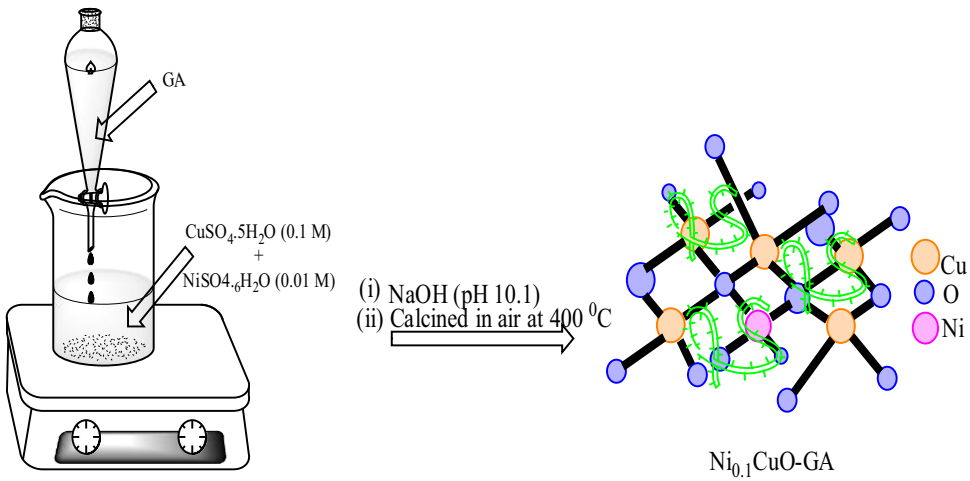

Scheme 1 Schematic diagram for the synthesis of $Ni_{0.1}CuO$-GA

Table 1 Optimization of the synthesis of $Ni_{0.1}CuO$-GA (30 mL of GA solution of different concentrations were used at fixed concentrations (0.1 M) of $CuSO_4$ and (0.01 M) of $NiSO_4$

S. No.	$CuNi_{0.1}$-GA Sample	GA % (w/v)	Yield (mg)
1.	G_1	0.50	381.7
2.	G_2	1.00	390.2
3.	G_3	1.50	396.4
4.	G_4	2.00	401.5

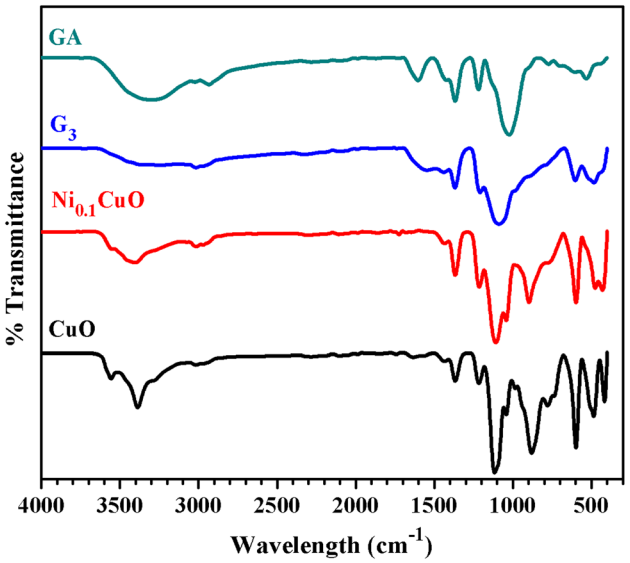

Fig. 1 FTIR spectra of GA, G_3, $Ni_{0.1}CuO$ and CuO

CuO-GA peaks associated to GA and CuO both are visible (spectrum not shown).

In FTIR spectrum of $Ni_{0.1}CuO$, the characteristic peaks of Cu–O shifted to 420 cm^{-1} and 480 cm^{-1} while the peak at 598 cm^{-1} retained its position. The shifts due to Ni doping may be assigned to the surface related defects. In FTIR spectra of CuO and $Ni_{0.1}CuO$, broad band observed at 3300–3600 cm^{-1} can be ascribed to the vibrations of the physically adsorbed water molecules.

In FTIR spectrum of G_3, the peaks due to O–H and C–H stretching vibrations are seen shifted to 3383 cm^{-1} and 3017 cm^{-1} respectively. The characteristic peaks of Cu–O shifted to 482 cm^{-1} and 602 cm^{-1}. The asymmetric and symmetric stretching vibrations of COO^- are seen shifted to 1561 cm^{-1} and 1428 cm^{-1} respectively. The shifts in the peak due to Ni doping and GA capping may be associated to the surface related defects [32].

Figure 2 presents room temperature UV–visible spectra of CuO, $Ni_{0.1}CuO$ and G_3. The spectra of CuO, $Ni_{0.1}CuO$ and G_3 showed broad absorption peaks entered at 257 nm, 255 nm and 242 nm respectively. The band gaps for CuO,

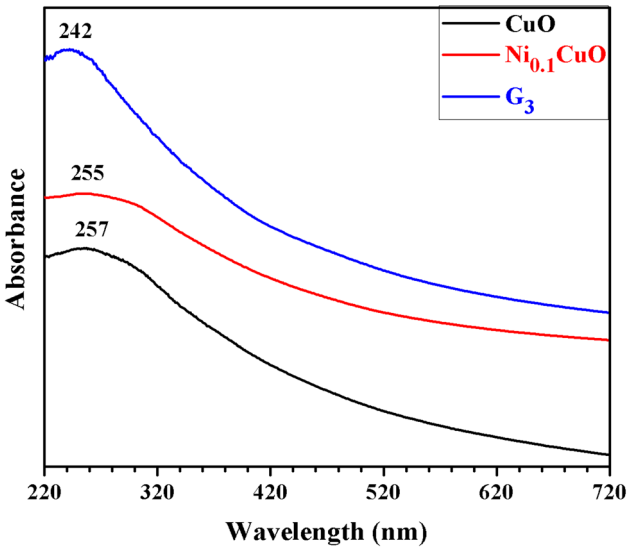

Fig. 2 UV-visible spectra of CuO, $Ni_{0.1}CuO$ and G_3 nanostructures

$Ni_{0.1}CuO$ and G_3 nanostructures have been calculated as 2.19, 2.60, and 2.73 respectively. Thus it is evident that both the Ni doping and GA capping have increased the band gap of CuO nanostructures. This can also be explained in terms of particle size which decreased by Ni doping and GA capping. The reduction in particle size leads to the well-known quantum confinement effect of semiconductors. Another study [35] has also reported similar observation where Ni doping decreased the band gap of CuO nanostructures and improved their photostability.

The XRD patterns of G_1-G_4 and the controls (CuO-GA, CuO and $Ni_{0.1}CuO$) are depicted in Fig. 3(i) and 3(ii) respectively. CuO showed sharp crystalline peaks at 2θ 33.29°, 35.69°, 38.82°, 46.27°, 48.79°, 52.91°, 58.33°, 61.66°, 66.20°, 68.15° and 72.39° which conform to monoclinic crystalline form of CuO [30]. The observed peaks can be assigned for the (−110), (002), (111), (−112), (−202), (020), (202), (−113), (−311), (−220) and (311) planes (respectively) of the monoclinic structure of CuO (JCPDS card no 45-0937). Ni-doping did not affect the monoclinic structure of CuO where as it affected the overall crystallinity of the samples, which can be inferred from the decrease in the intensity of the peaks of $Ni_{0.1}CuO$. In $Ni_{0.1}CuO$ the crystalline peaks are seen 2θ at 33.11°, 35.84°, 38.58°, 46.20°, 48.81°, 52.74°, 61.85° and 66.01°. In $Ni_{0.1}CuO$, no nickel oxide diffraction peak is observed that indicated that Ni doping did not change the crystalline structure of CuO, however the diffraction peaks of the $Ni_{0.1}CuO$ displayed a slight shift to angles as Ni was incorporated into the CuO lattice. An efficient substitution of Ni^{2+} for Cu^{2+} was possible as the ionic radius of Ni^{2+} (0.69 A°) is smaller than Cu^{2+} (0.73 A°). This substitution instigated a minor lattice reduction of the CuO matrix [46].

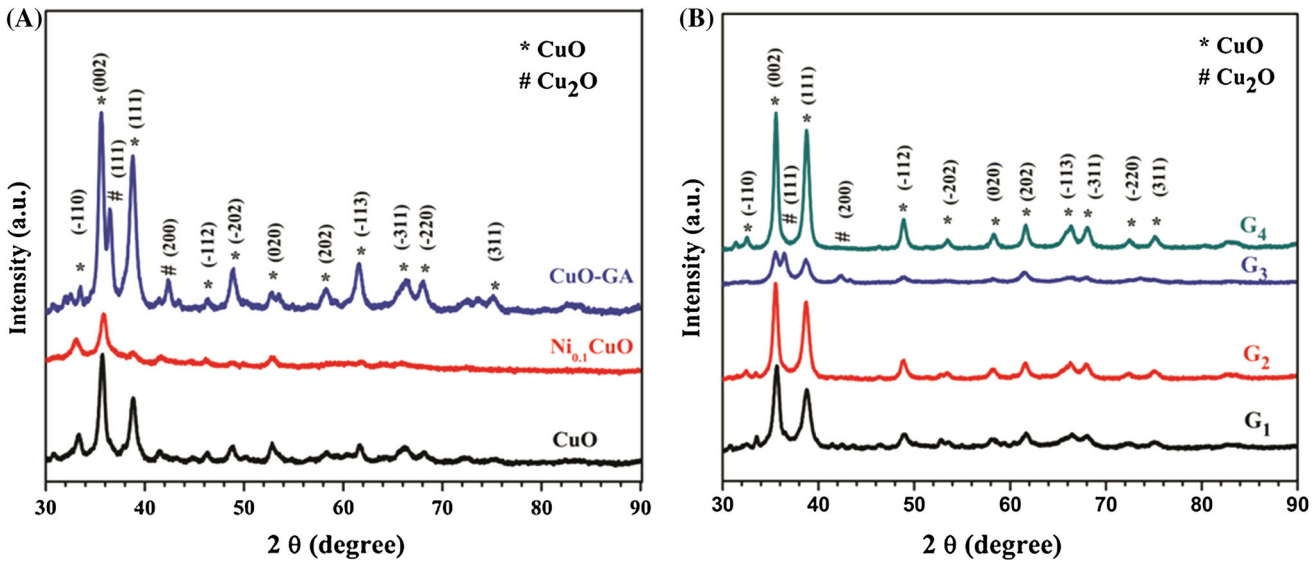

Fig. 3 XRD patterns **a** CuO-GA, $Ni_{0.1}CuO$, CuO **b** G_1, and G_2, G_3, G_4 nanostructures

The reduction in crystallite size of Ni doped CuO sample may be assigned to the distortion in crystalline structure of CuO. In G_3, the crystalline peaks of CuO are seen 2θ at 35.50°, 38.70°, 48.88°, 53.43°, 58.21°, 61.54°, 66.35°, 67.95° and 73.59°. A diffraction pattern of the Cu_2O cubic phase (JCPDS card no 05-0667) is also visible at 2θ 36.4° (Cu_2O (111) crystal plane), and 42.35° [47]. This indicated a small contamination of Cu_2O phase in G_3 sample. Similarly CuO-GA sample showed sharp crystalline peaks matching with the monoclinic structure of CuO (at 2θ 35.6°, 38.76°, 48.84°, 58.25°, 61.6°, 66.29° and 68.03°) along with peaks of Cu_2O cubic phase (at 2θ 36.38° and 42.38°). The average crystallite size of CuO-GA is 9.23 nm. It is evident that in samples G_3 and CuO-GA, small amount of Cu_2O phase exist along with CuO while rest of the samples G_1, G_2, G_4 did not show any peaks associated with Cu_2O. It may be inferred that during calcination GA has reduced some CuO to Cu_2O phase [48].

Thus GA has manipulated the crystalline phase of the copper oxide. In many previous reports GA has shown reducing and capping behavior [49].

The average particle sizes (as calculated by Scherrer's equation) of CuO, $Ni_{0.1}CuO$ and G_3 are 15.5 nm, 12.07 nm and 8.8 nm respectively. This trend indicates that Ni doping and GA capping has decreased the average crystallite size of the CuO nanostructures.

FESEM images of G_1 to G_4, $Ni_{0.1}CuO$, CuO-GA and CuO are shown in the Fig. 4. The images gave clear cut evidence of change in CuO morphology on Ni doping and using GA as growth medium. CuO-GA and CuO showed cluster of needle like particles where the size of the particles in CuO are rather smaller while on same magnification $Ni_{0.1}CuO$ showed flattened layered morphology. G_3 on the other hand showed fluffy morphology constituted of small spherical particles. The morphologies of G_1 to G_3 are almost similar except G_3 has finer particles. G_4 has quite different morphology than samples G_1 to G_3 which is consistent with its lesser efficacy as antibacterial material. Its particles are clustered to form layered flower like structure Fig. 5 (i) and (ii) clearly confirmed the Ni doping to CuO in the samples G_1–G_4 and $Ni_{0.1}CuO$.

The morphology of G_3 was also examined by HR-TEM (Fig. 6). HR-TEM image revealed nearly spherical shape of G_3 nanoparticles which are seen clustered at places. The material's crystalline nature is evident from the SAED pattern (inset of Fig. 6b)) which showed sharp fringes. The HRTEM images of G_3 at different magnifications are shown in Fig. 6a, b. The images revealed that average particle size of G_3 is ∼ 12 nm (Histogram image 6c). It appears that one nanoparticle is constituted of several crystalline domains of smaller size (Fig. 6).

Antibacterial Activity

Antibacterial properties of G_3 was studied for gram positive (*S. aureus*) and gram negative (*P. aeruginosa*, *E. aerogenes, K. pneumoniae*) bacterial strains. Among the tested bacterial strains, all the samples (ranging from G_1 to G_4) were more bioactive than CuO Nps and $Ni_{0.1}CuO$ nanoparticles (Table 2). Neat GA did not exhibit any antibacterial activity. The antibacterial performance was tested for 5 mg/mL dose of materials and the results are presented in Table 2 and Fig. 7.

It is evident from Table 2 that the samples G_1 to G_4 were much more active than the antibiotic (Ampicillin)

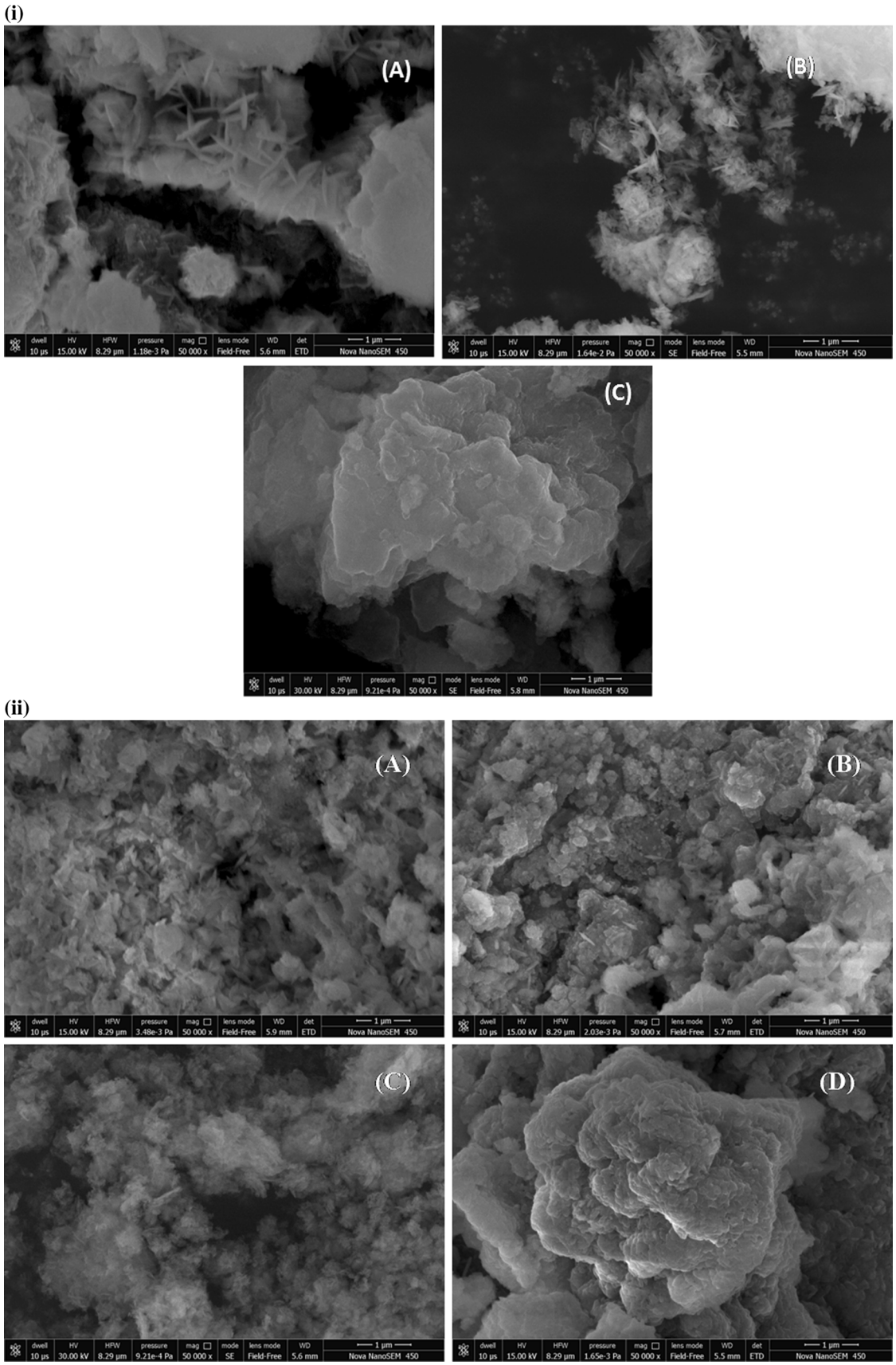
(i)
(A)
(B)
(C)
(ii)
(A)
(B)
(C)
(D)

◀**Fig. 4** (**i**) FESEM image of **a** GA-CuO; **b** CuO **c** $Ni_{0.1}CuO$ at 50,000x magnification, (**ii**) FESEM image of **a** G_1; **b** G_2 **c** G_3 **d** G_4 at 50,000x magnification

while $Ni_{0.1}CuO$ and CuO had almost equal efficacy for the tested strains but both are less active than $Ni_{0.1}CuO$-GA samples (G_1–G_4). Among $Ni_{0.1}CuO$-GA samples, G_3 is most active (Table 2). GA is an acidic polysaccharide having carboxyl functional groups which offer opportunity for creating extra oxygen vacancies for generating extra free radicals, as GA content increased this effect increased while beyond 1.5% (w/v) GA, the performance slightly decreased as now excess of GA masks the active sites of CuO nanostructures.

The antimicrobial efficacy of synthesized samples (CuO, $Ni_{0.1}CuO$ and $Ni_{0.1}CuO$-GA nanoparticles) was studied against four bacterial strains which are known to have serious life-threatening effects. *Enterobacter aerogenes* is important opportunistic and multi-resistant pathogen and has emerged as noscomoial pathogen in intensive care unit patients, especially for patients on mechanical ventilation [50]. *Klebsiella* infects respiratory tract and causes pneumoniae. *Klebsiella* infections are contagious [51]. *Pseudomonas aeruginosa* is responsible for many hospital-acquired serious infections [52]. *Staphylococcus aureus* is a human pathogen that is responsible for a wide range of clinical infections such as bacteremia, infective endocarditis as well as osteoarticular, skin and soft tissue, pleuropulmonary, and device-related infections [53]. Among (CuO, $Ni_{0.1}CuO$ and $Ni_{0.1}CuO$-GA), $Ni_{0.1}CuO$-GA samples were more active against the both, Gram-negative and Gram-positive bacteria.

The $Ni_{0.1}CuO$-GA nanocomposite samples (G_1 to G_4) are especially effective against *K. pneumoniae* and *P. aeruginosa*. Sample G_3 (0.5 mg/mL) exhibited 28.75 mm zone of inhibition diameter for *K. pneumoniae* and 27.50 mm for *P. aeruginosa*. The zone of inhibition diameter of G_3 for *E. aerogenes* and *S. aureus* are 27 mm and 26.50 mm respectively. The antibacterial activity of G_3 for *K. pneumoniae* and *P. aeruginosa* is quite attractive as its low dose could create significantly high zone of inhibition that exceeded even Ampicillin, the reference antibiotic. ZOI for CuO-GA against *E. aerogenes*, *K. pneumoniae*, *P. aeruginosa*, *S. aureus* bacterial strains was found to be 24.3, 25.7, 24.8 and 23.9 mm respectively which are greater than CuO, $Ni_{0.1}CuO$ and the control antibiotic. This sample has contamination of Cu_2O phase as that of G_3 but its efficacy is almost similar to samples G_1, G_2, and G_4 which exhibited pure monoclinic CuO phase. Thus antibacterial activity is not dictated by phase of copper oxide rather it is a specific combination of Ni doping and GA concentration. These results indicated that Ni doping and GA inclusion both have an important role in designing the efficient antibacterial material and GA at 1.5% (w/v) concentration furnished the most effective material. In present study samples G_3 and CuO-GA have shown small contamination of Cu_2O phase while samples CuO, G_1, G_2, and G_4 have pure CuO crystalline phase. The presence of GA tailored the crystalline phase of the copper oxide nanostructures. GA has shown reducing and capping behaviour in synthesizing the nanostructures in many previous reports [49]. In absence of GA, the CuO nanostructures are formed while the presence of GA led to reduction of CuO as Cu_2O which are also stabilized by GA. However in G_4, where concentration of GA is high (2% w/v) no formation of Cu_2O phase is witnessed. This indicated that high GA concentration, polysaccharide molecules self associates and are not free for reducing the CuO nanostructures rather some of the active sites of the material were masked by excess GA. The antibacterial behavior of samples revealed that inclusion of Cu_2O phase and Ni doping combined with adequate GA concentration (1.5% (w/v) furnish excellent antibacterial material. Literature reveals that CuO nanoparticles synthesized from other routes required either higher dose or exhibited lower diameter of zone of inhibition, e.g., Ahamed et al. have reported CuO nanoparticles whose 500 μg mL^{-1} dose could furnish ZOI diameter between 5 and 10 mm for *K. Pneumoniae* and *P. aeruginosa* [54]. In another report, CuO nanosheets (10 mg/mL) showed 9.0 mm zone of inhibition diameter for *P. aeruginosa* [5]. Table **3** summarizes antibacterial activity of some of previously reported CuO materials for reference.

The small sizes, thus large surface areas of $Ni_{0.1}CuO$-GA samples make them highly bioactive. The small size is the result of GA capping and Ni doping to CuO nanostructures. The distinctive high surface to volume ratio of copper nanoparticles permits them to interact with the cell membrane of the bacteria through its surface, resulting in the death of bacteria [55].

The antibacterial activities of $Ni_{0.1}CuO$-GA samples were higher for gram-negative bacteria in comparison to gram-positive bacteria. This difference can be attributed to thicker peptidoglycan cell membrane of gram positive bacteria and thus it is harder to penetrate [56].

As the GA component was increased (from 0.5% to 2%) in $Ni_{0.1}CuO$-GA samples, their inhibitory activity increased (G_1 to G_3) for the tested strains of bacteria, while for G_4 sample it was marginally lower. This trend is expected as when less GA was associated with the samples, less number of CuO nanoparticles were formed which is also evident from TEM studies. When 1.5% (w/v) GA was used for $Ni_{0.1}CuO$-GA synthesis, a sufficient number of ZnO-GA nanoparticles were generated because population of the capping GA molecules was increased to produce

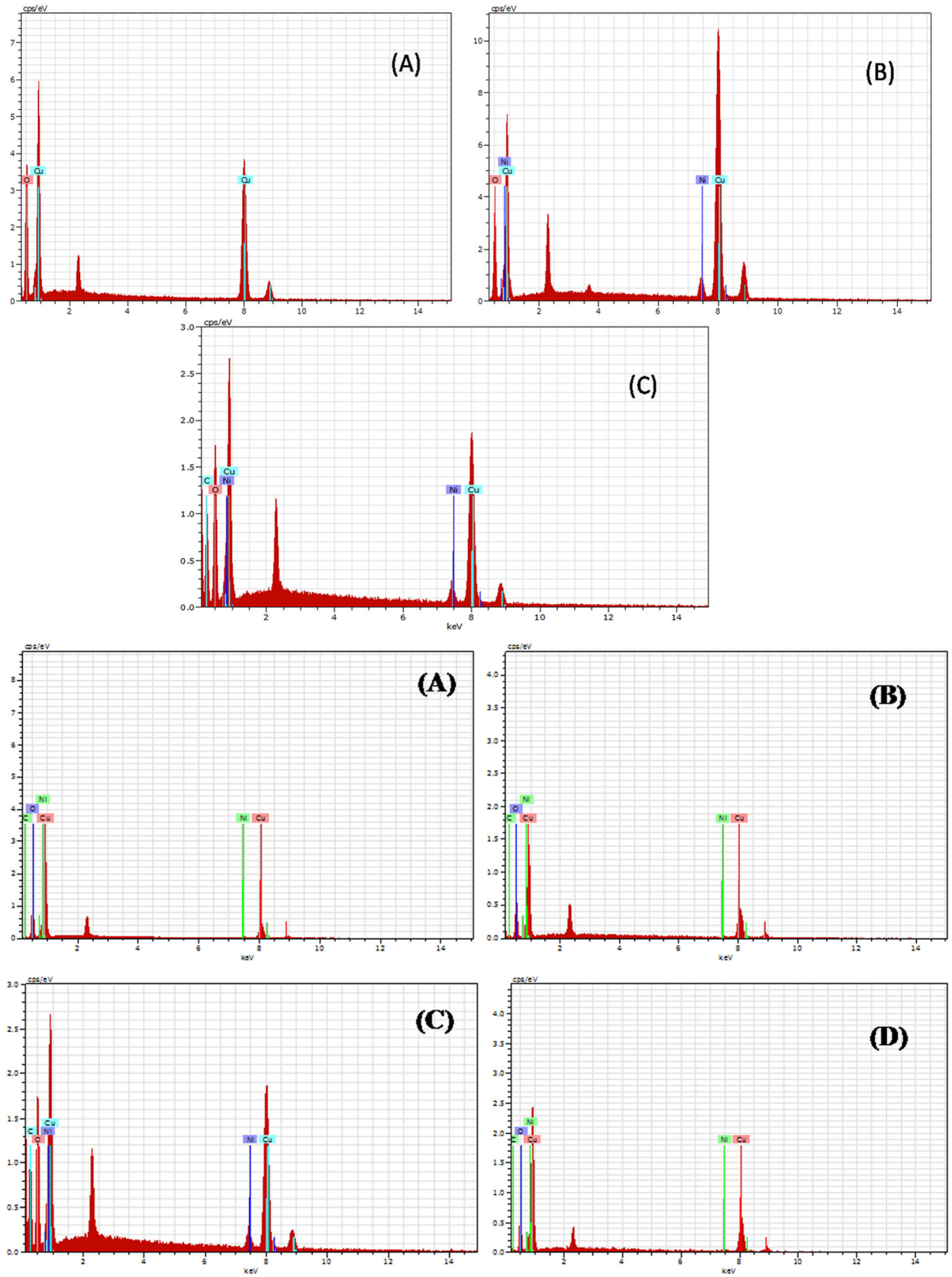

Fig. 5 (**i**) EDAX of **a** CuO, **b** $Ni_{0.1}CuO$ and **c** G_3, (**ii**) (i) EDAX of **a** G_1 **b** G_2 and **c** G_3 **d** G_4

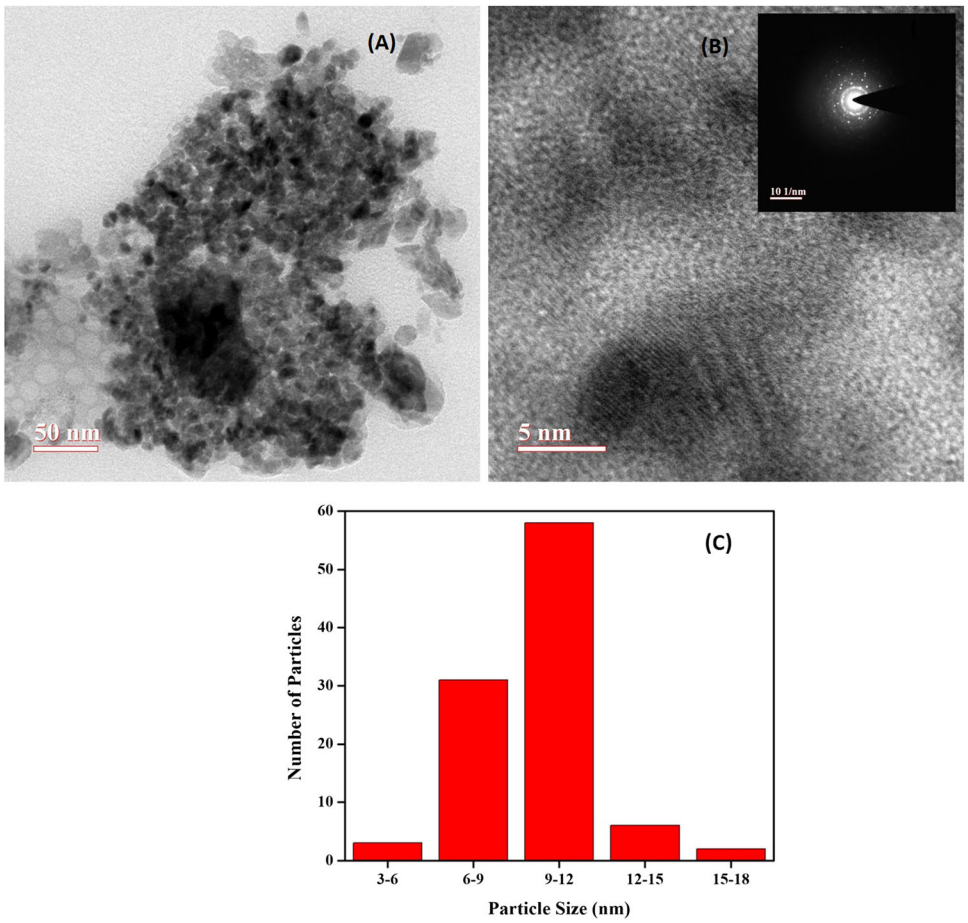

Fig. 6 **a** and **b** HR-TEM image of G_3 **c** Histogram of size distibution of G_3

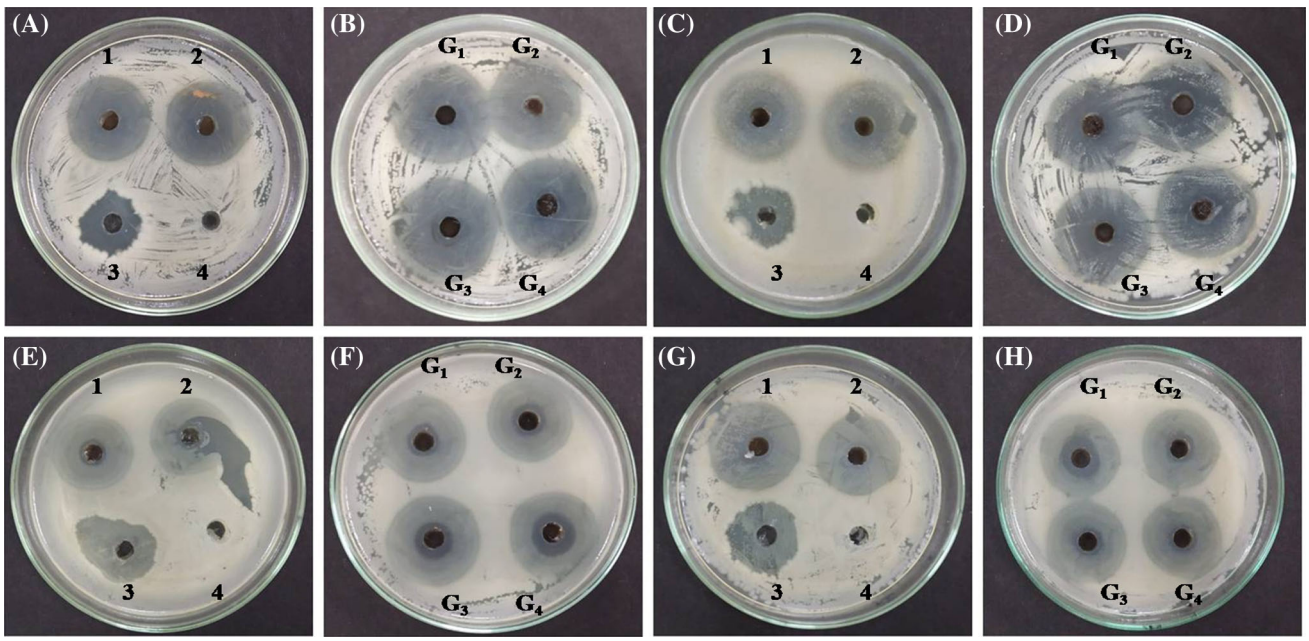

Fig. 7 Details of antibacterial study: **a**, **b** = Enterobacter, **c**, **d** = *K. pneumoniae*, **e**, **f** = *P. aeruginosa*, **g**, **h** = *S. aureus*; 1 = CuO, 2 = $Ni_{0.1}CuO$, 3 = Ampicillin, 4 = Sterilized distilled water; G_1 = $Ni_{0.1}CuO$-GA (0.50%), G_2 = $Ni_{0.1}CuO$-GA (1.0 %), G_3 = $Ni_{0.1}CuO$-GA (1.5 %), G_4 = $Ni_{0.1}CuO$-GA (2.0 %)

Table 2 Antibacterial activity for different bacterial strains at 5 mg/mL dose (zone of inhibition diameter in mm)

S. No.	Bacterial strains	$Ni_{0.1}CuO$-GA				CuO	$Ni_{0.1}CuO$	Antibiotic (Ampicillin)
		G_1	G_2	G_3	G_4	1	2	3
1.	*Enterobacter*	24.50	25.25	27.00	24.50	22.00	22.50	17.50
2.	*K. pneumoniae*	24.75	25.00	28.75	25.50	24.00	24.00	18.50
3.	*P. aeruginosa*	23.25	25.25	27.50	24.50	20.50	21.50	18.25
4.	*S. aureus*	25.0	24.25	26.50	24.25	22.50	21.75	19.00

Table 3 Antibacterial activity of some of previously reported materials in comparison to the present materials

S. no.	Morphology	Method of preparation	Bacteria	Important results	Ref.
1.	Nanosheets	Reflux condensation method	*P. aeruginosa*	ZOI = 9 mm (ZOI for 10 mg mL^{-1} for the strain)	[5]
3.	Nanoparticles	Precipitation method	*P. aeruginosa*	ZOI = Between 5 and 10 mm	[54]
			K. pneumoniae	ZOI = Between 5 and 10 mm	
			S. aureus	ZOI = Between 10 and 15 mm (ZOI for 500 μg mL^{-1} for all strain)	
5.	Nanoparticles	Green synthesis of CuO nanoparticles using *Syzygium alternitolium* stem bark	*S. aureus*	ZOI = Between 5 and 10 mm	[58]
			P. aeruginosa	(ZOI for 80 μg mL^{-1} for both strains)	
2.	Nanoparticles	Biosynthesis of CuO nanoparticles using brown algge extract (*Bifurcaria bifurcata*)	*S. aureus*	ZOI = 16 mm	[59]
			Enterobacter	ZOI = 14 mm	
4.	Colloidal nanoparicles	Pulsed laser ablation method	*S. aureus*	Inhibition rate 11.7% and 19.5%	[60]
			P. aeruginosa	(Inhibition rate of CuO nanoparticles at a concentration of 1000 μg mL^{-1} for both strains)	
6.	Nanoparticles	Biosynthesis of CuO nanoparticles using actinomycetes	*S. aureus*	ZOI = 19.6 ± 0.57 mm (ZOI for 100 μg mL^{-1} for the strain)	[61]
7.	Nanoparticles (G_3)	Co–precipitation method	*Enterobacter,*	ZOI = 27 mm,	Present work
			K. pneumoniae	ZOI = 28.75 mm,	
			P. aeruginosa	ZOI = 27.50 mm,	
			S. aureus	ZOI = 26.50 mm (ZOI for 500 μg mL^{-1} for all strain)	

smaller particles. Small particles can easily adhere to the cell wall of the microorganisms and cause its destruction which ultimately leads to death of the cell [57].

Conclusion

$Ni_{0.1}CuO$-GA has been obtained by 0.1 mol Ni doping to CuO Nps in presence of gum acacia polysaccharide. The material showed excellent antibacterial property. It was more effective antibacterial material than antibiotic (Amplicillin) and simple Ni doped CuO Nps control and CuO-GA samples. ZOI for *Enterobacter, Klebsiella pneumoniae, Pseudomonas aeruginosa* and *Staphylococcus aureus* were 27 mm, 28.75 mm, 27.50 mm and 26.50 mm in comparison to ZOI for the reference antibiotic which was 17.50 mm, 18.50 mm, 18.25 mm and 19.50 mm respectively with a dose of 5 mg/ml of G_3. For neat CuO Nps, CuO-GA and Ni doped CuO ($Ni_{0.1}CuO$) ZOI ranged between 21 and 24 mm for the same doses. Thus inclusion of GA as growth medium for the synthesis of Ni doped CuO nanoparticles had a clear cut advantage in terms of antibacterial property of the material obtained thereof.

Acknowledgements Authors thanks MNNIT, Allahabad for XRD facility. MNIT, Jaipur is acknowledged for FTIR, SEM and TEM instrumental facilities. Author LMD thank U.G.C, New Delhi for the financial support to carry out this work.

References

1. S. Pandey (2016). *J. Sci.* **1**, 431.
2. G.A. Ozin, A.C. Arsenault, and L. Cademartiri (2008). *R Soc Chem*.
3. L. Argueta-Figueroa, R. A. Morales-Luckie, R. J. Scougall-Vilchis, and O. F. Olea-Mejía (2014). *Proc. Nat. Sci. Mater.* **24**, 321.

4. R. García Contreras, L. Argueta Figueroa, C. Mejía Rubalcava, R. Jiménez Martínez, S. Cuevas Guajardo, P. A. Sánchez Reyna, and H. Mendieta Zeron (2011). *Int. Dent. J.* **61**, 297.
5. R. Sathyamoorthy and K. Mageshwari (2013). *Phys. E* **47**, 157.
6. S. Reddy, B. K. Swamy, and H. Jayadevappa (2012). *Electrochim. Acta* **61**, 78.
7. C. T. Hsieh, J. M. Chen, H. H. Lin, and H. C. Shih (2003). *Appl. Phys. Lett.* **83**, 3383.
8. D. Su, X. Xie, S. Dou, and G. Wang (2014). *Sci. Rep.* **4**, 5753.
9. P. K. Singh, A. K. Das, G. Hatui, and G. C. Nayak (2017). *Mater. Chem. Phys.* **198**, 16.
10. M. M. Rashad, D. A. Rayan, and A. A. Ramadan (2013). *J. Mater. Sci. Mater. Electron* **24**, 2742.
11. J. Linnera, G. Sansone, L. Maschio, and A. J. Karttunen (2018). *J. Phys. Chem. C* **122**, 15180.
12. M. Dahrul, H. Alatas, and H. Irzaman (2016). *Procedia Environ. Sci.* **33**, 661.
13. Z. Zhou, C. Lu, X. Wu, and X. Zhang (2013). *RSC Adv.* **3**, 26066.
14. A. S. Reddy, H. H. Park, V. S. Reddy, K. V. Reddy, N. S. Sarma, S. Kaleemulla, S. Uthanna, and P. S. Reddy (2008). *Mater. Chem. Phys.* **110**, 397.
15. L. Chen, S. Shet, H. Tang, H. Wang, T. Deutsch, Y. Yan, J. Turner, and M. Al-Jassim (2010). *J. Mater. Chem.* **20**, 6962.
16. A. Chen, H. Long, X. Li, Y. Li, G. Yang, and P. Lu (2009). *Vacuum* **83**, 927.
17. N. H. Hung, N. D. Thanh, N. H. Lam, N. D. Dien, N. D. Chien, and D. D. Vuong (2014). *Mater. Sci. Semicond. Process* **26**, 18.
18. N. R. Dhineshbabu, V. Rajendran, N. Nithyavathy, and R. Vetumperumal (2016). *Appl. Nanosci.* **6**, 933.
19. N. M. Basith, J. J. Vijaya, L. J. Kennedy, and M. Bououdina (2014). *Mater. Sci. Semicond. Process* **17**, 110.
20. J. Jayaprakash, N. Srinivasan, and P. Chandrasekaran (2014). *Spectrochim. Acta Part A* **123**, 363.
21. P. Arunachalam, S. Nagarani, S. Prasad, M. S. AlSalhi, A. M. Al-Mayouf, and S. Ganapathy (2018). *Mater. Res. Express* **5**, 015512.
22. R. Sasikala, S. K. Rani, K. Karthikeyan, and D. Easwaramoorthy (2016). *J. Eng. Chem. Fuel* **1**, 43.
23. S. Meghana, P. Kabra, S. Chakraborty, and N. Padmavathy (2015). *RSC Adv.* **5**, 12293.
24. P. Mantecca, E. Moschini, P. Bonfanti, U. Fascio, I. Perelshtein, A. Lipovsky, G. Chirico, R. Bacchetta, L. Del Giacco, A. Colombo, and A. Gedanken (2015). *Toxicol. Sci.* **146**, 16.
25. M. Grigore, E. Biscu, A. Holban, M. Gestal, and A. Grumezescu (2016). *Pharmaceuticals* **9**, 75.
26. V. Singh, L. M. Dwivedi, K. Baranwal, S. Asthana, and S. Sundaram (2018). *Appl. Nanosci.* **8**, 1149.
27. V. Vellora, T. Padil, and M. Černík (2013). *Int. J. Nanomed.* **8**, 889.
28. S. Masudy-Panah, K. Radhakrishnan, H. R. Tan, R. Yi, T. I. Wong, and G. K. Dalapati (2015). *Sol. Energy. Mater. Sol. Cells* **140**, 266.
29. A. A. Oliveira, M. I. Valerio-Cuadros, L. F. S. Tupan, F. F. Ivashita, and A. Paesano Jr. (2018). *Mater. Lett.* **229**, 327.
30. Y. Wang, T. Jiang, D. Meng, D. Wang, and M. Yu (2015). *Appl. Surf. Sci.* **355**, 191.
31. M. Eshed, J. Lellouche, A. Gedanken, and E. Banin (2014). *Adv. Funct. Mater.* **24**, 1382.
32. R. N. Mariammal, K. Ramachandran, G. Kalaiselvan, S. Arumugam, B. Renganathan, and D. Sastikumar (2013). *Appl. Surf. Sci.* **270**, 545.
33. X. Bai, W. Chen, Y. Song, J. Zhang, R. Ge, W. Wei, Z. Jiao, and Y. Sun (2017). *Appl. Surf. Sci.* **420**, 927.
34. S. Dolai, S. N. Sarangi, S. Hussain, R. Bhar, and A. K. Pal (2019). *J. Magn. Magn. Mater.* **479**, 59.
35. J. Oh, H. Ryu, W. J. Lee, and J. S. Bae (2018). *Ceram. Int.* **44**, 89.
36. A. E. A. Morsy, M. Rashad, N. M. Shaalan, and M. A. Abdel-Rahim (2019). *Micro Nanosyst.* **11**, 109.
37. P. Debashri and N. Sudarsan (2019). *Mater. Res. Express* **6**, 055004.
38. L. Arun, C. P. Karthikeyan, D. D. Dhayanithi, and N. V. Giridharan (2018). C, Unni. *Opt .Quant. Electron* **50**, 414.
39. C. Thangamani, M. Ponnar, P. Priyadharshini, P. Monisha, S. S. Gomathi, and K. Pushpanathan (2019). *Surf. Rev. Lett.* **26**, 1850184.
40. S. Al-Amri, M. Shahnawaze Ansari, S. Rafique, M. Aldhahri, S. Rahimuddin, A. Azam, and A. Memic (2015). *Curr. Nanosci.* **11**, 191.
41. S. Pandey and J. Romantja (2016). *Int. J. Biol. Macromol.* **93**, 712.
42. V. Singh and S. Ahmed (2012). *Int. J. Biol. Macromol.* **50**, 353.
43. V. Singh, A. K. Pandey, J. Singh, and T. Malviya (2016). *RSC Adv.* **6**, 31074.
44. K. Borgohain, J. B. Singh, M. R. Rao, T. Shripathi, and S. Mahamuni (2000). *Phys. Rev. B* **61**, 11093.
45. A. Sahai, N. Goswami, and S. D. Kaushik (2016). S. Tripathi. *Appl. Surf. Sci.* **390**, 974.
46. K. Matsubara, S. Huang, M. Iwamoto, and W. Pan (2014). *Nanoscale* **6**, 688.
47. V. Cretu, V. Postica, A. K. Mishra, M. Hoppe, I. Tiginyanu, Y. K. Mishra, L. Chow, N. H. de Leeuw, R. O. Adelung, and O. Lupan (2016). *J. Mater .Chem. A* **4**, 6527.
48. S. S. Sawant, A. D. Bhagwat, C. M. Mahajan, J. Nano Electron. Phys. V 8, 01035(5 pp) (2016).
49. D. K. Devi, S. V. Pratap, R. Haritha, K. S. Sivudu, P. Radhika, and B. Sreedhar (2011). *J. Appl. Polym. Sci.* **121**, 1765.
50. M. L. Mezzatesta, F. Gona, and S. Stefani (2012). *Future Microbiol.* **7**, 887.
51. Y. Ma, C. Bao, J. Liu, X. Hao, J. Cao, L. Ye, and J. Yang (2018). *J. Glob. Antiomicrob. Resist.* **12**, 162.
52. J. A. Colmer-Hamood, N. Dzvova, C. Kruczek, and A. N. Hamood (2016). *Progress Mol. Biol. Trans. Sci.* **142**, 151.
53. S. Y. Tong, J. S. Davis, E. Eichenberger, T. L. Holland, and V. G. Fowler (2015). *Clin. Microbiol. Rev.* **28**, 603.
54. M. Ahamed, H. A. Alhadlaq, M. A. Khan, P. Karuppiah, and N. A. Al-Dhabi (2014). *J. Nanomater.* **2014**, 17.
55. M. S. Usman, M. E. El Zowalaty, K. Shameli, N. Zainuddin, M. Salama, and N. A. Ibrahim (2013). *Int. J. Nanomed.* **8**, 4467.
56. J. S. Tawale, K. K. Dey, R. Pasricha, K. N. Sood, and A. K. Srivastava (2010). *Thin Solid Films* **519**, 1244.
57. M. Sulochana, C. S. Vani, D. K. Devi, N. S. Naidu, and B. Sreedhar (2013). *Am. J. Mater. Sci.* **3**, 169.
58. P. Yugandhar, T. Vasavi, P. U. Devi, and N. Savithramma (2017). *Appl. Nanosci.* **7**, 417.
59. Y. Abboud, T. Saffaj, A. Chagraoui, A. El Bouari, K. Brouzi, O. Tanane, and B. Ihssane (2014). *Appl. Nanosci.* **4**, 571.
60. K. S. Khashan, G. M. Sulaiman, and F. A. Abdulameer (2016). *Arab. J. Sci. Eng.* **41**, 301.
61. M. I. Nabila and K. Kannabiran (2018). *Biocatal. Agric. Biotechnol.* **15**, 56.